

Article

Chemical Characterization of Waterlogged Charred Wood: The Case of a Medieval Shipwreck

Eirini Mitsi ¹, Stamatis Boyatzis ² and Anastasia Pournou ^{2,*}

¹ Department of History, Archaeology and Cultural Resources Management, University of the Peloponnese, 24100 Kalamata, Greece; eir.mitsi@gmail.com

² Department Conservation of Antiquities & Works of Art, University of West Attica, Ag. Spyridonos Str., Aegaleo, 12243 Athens, Greece; sboyatzis@uniwa.gr

* Correspondence: pournou@uniwa.gr

Abstract: In 2008, a medieval wooden shipwreck was discovered at the port of Rhodes, Greece. The shipwreck was partly burned, presenting a challenge for conservators, as uncharred, semi-charred and charred waterlogged wood were often encountered on the same piece of timber. In seeking the most appropriate conservation method for this unusual material, its chemical characterization was considered necessary. This study examined the chemistry of the three dominant wood conditions found in the wreck. Fourier transform infrared spectroscopy and X-ray diffraction analysis were implemented in comparison to reference samples. Energy dispersive analysis was also used for assessing the inorganic composition of each condition. Moreover, for charred and semi-charred wood, proximate analysis was undertaken. Results obtained regarding the organic moieties of the waterlogged archaeological material, demonstrated that charred samples were chemically comparable to charcoals, semi-charred material showed similarity to thermally modified wood, whereas uncharred waterlogged wood was proven to have an analogous chemistry to biodeteriorated wood. Elemental analysis results also diversified among the three shipwreck's conditions. Sulfur, iron, and oxygen decreased in charred areas, whereas carbon increased. Proximate analysis showed that ash and fixed carbon content increased with charring, whereas volatile matter decreased. This work proved major chemical differences among shipwreck timbers' conditions owing to different degree of charring. These are anticipated to influence not only conservation methods' efficacy, but also the post-treatment behavior of the material. Further investigation is needed for correlating the chemistry of the archaeological material to its physical properties in order to contribute to practical aspects of conservation.

Keywords: medieval shipwreck; waterlogged wood; charred wood; chemical analysis; EDS; FTIR; XRD; proximate analysis



Citation: Mitsi, E.; Boyatzis, S.; Pournou, A. Chemical Characterization of Waterlogged Charred Wood: The Case of a Medieval Shipwreck. *Forests* **2021**, *12*, 1594. <https://doi.org/10.3390/f12111594>

Academic Editors: Magdalena Broda and Callum A. S. Hill

Received: 9 October 2021

Accepted: 17 November 2021

Published: 19 November 2021

Publisher's Note: MDPI stays neutral with regard to jurisdictional claims in published maps and institutional affiliations.



Copyright: © 2021 by the authors. Licensee MDPI, Basel, Switzerland. This article is an open access article distributed under the terms and conditions of the Creative Commons Attribution (CC BY) license (<https://creativecommons.org/licenses/by/4.0/>).

1. Introduction

During a routine survey in 2008, a late-12th-century ship was discovered at the commercial port of Rhodes by the Greek Ephorate of Underwater Antiquities [1,2]. The shipwreck lay at a maximum depth of 13–14 m and was found half-buried in muddy sediment [1].

In 2013, a partial excavation of the shipwreck revealed that it was a merchant ship loaded with a cargo of amphorae and made apparent that a fire event took place before the vessel sunk [1]. Extensive or superficial traces of burning were recorded on many constructional elements of the ship, such as frames, ceiling planking, and stringers, and almost on every artifact recovered [1,2].

Excavated wooden hull members, identified as *Pinus halepensis* Mill. or *Pinus brutia* Ten. [1], showed a varied preservation state, as the degree and depth of charring was not homogenous among ship timbers due to the fire progression [3]. The coexistence of uncharred, semi-charred, and charred wood, often encountered on the same timber,

poses a great challenge for the ship's future conservation as wood responds differently to impregnation and drying, depending on its charring degree [3]. However, literature on the conservation of waterlogged charred wood is scarce and there are no studies associating the conservation requirements with material's physical and chemical properties. Nonetheless, it is well known that thermal decomposition of wood is accompanied by major chemical changes in hygroscopicity, viscosity, cell wall structure, color, density, and loss of mass and strength [4–8]. Moreover, it is also documented that these alterations depend on variables related not only on the wood, such as density, moisture content, permeability, species, size, grain direction, and surface protection [7,9], but also on the heating scenario, which incorporates the heat flux (temperature and duration) and the environment surrounding the wood like the oxygen concentration [7,9–13]. All these factors which influence pyrolysis, combustion, and the charring rate of wood justify the coexistence of charred, semi-charred, and uncharred wood in the shipwreck.

Preliminary experiments undertaken for the conservation of this material with polyethylene glycol followed by air or freeze drying have demonstrated a very dissimilar response to consolidation [3]. This was rather anticipated because as wood reaches elevated temperatures, the thermally degraded structural and chemical components affect greatly its behavior [4–6,12,14].

Therefore, this study was set to characterize the chemistry of this dissimilarly charred material in order to help understand its behavior and provide insights towards the development of a successful conservation method.

2. Materials and Methods

Waterlogged wood examined in this study belonged to a wreck's frame made of *Pinus halepensis* Mill. (Aleppo pine) or *Pinus brutia* Ten. (Turkish pine) [1]. Part of the frame was retrieved in 2013, and was kept waterlogged at 5 °C until sampling. The material presented a varied degree of charring, as its outer surface was charred, its inner core was uncharred, and layers in between were semi-charred [3]. Samples used for the chemical characterization were taken from the surface inwards, at least 50 annual rings away from the pith, to correspond to the sapwood of the mature pine, and contained all three charring conditions.

2.1. Energy Dispersive Analysis (EDS)

Uncharred and semi-charred waterlogged archaeological samples were cut in subsamples using a double-edged razor blade, whereas charred samples were fractured. Subsamples were then dehydrated in a series of ethanol solutions of increasing concentrations until water-free alcohol was reached and left to air-dry in a desiccator. They were then mounted on aluminum stubs using a double coated carbon conductive tape and energy dispersive X-ray spectroscopy (EDS) was performed at an acceleration voltage of 20 kV under low vacuum (33 Pa) using a JEOL JSM-6510LV scanning electron microscope, equipped with an Inca x-act silicon drift detector (SDD) with PentaFET[®] Precision (Oxford Instruments, Oxford, UK). The analytical data were obtained with Inca[®] analysis software. Bulk analysis was applied on every wood condition, whereas line scans and mapping were applied on samples where all conditions coexisted.

2.2. Fourier Transform Infrared Spectroscopy (FTIR)

Uncharred, semi-charred, and charred waterlogged archaeological wood was air-dried, and along with sapwood of sound wood of mature *Pinus halepensis* Mill. and *Pinus brutia* Ten. were finely grounded manually with the use of an agate mortar and pestle to ~100 µm (No 140-mesh size). Wood powder was then mixed with potassium bromide powder (KBr, Merck), and pressed into 13 mm discs with a hydraulic press. Disc samples were placed in the FTIR system sample chamber for analysis.

All samples were analyzed with a Perkin Elmer Spectrum GX spectrometer, equipped with DTGS (deuterated diglycine sulfate) detector. Spectra were recorded and edited with the Perkin Elmer Spectrum v.5.3.1 software.

2.3. X-Ray Diffraction Analysis (XRD)

Air-dried uncharred, semi-charred, and charred, waterlogged archaeological samples along with sapwood of sound wood of mature *Pinus halepensis* Mill. and *Pinus brutia* Ten. were finely grounded manually with the use of an agate mortar and pestle to ~100 µm (No 140 mesh size).

X-ray diffraction spectra of wood powdered samples were recorded with the help of InXitu BTX II Benchtop X-ray Diffraction/X-ray Fluorescence hybrid system using a Cobalt source ($K\alpha_1$ 1.78897 Å). All spectra were recorded in duplicate after the completion of >1200 scan cycles from 5 to 50 degrees 2θ .

The crystallinity index (CrI) was calculated based on the method developed by Segal et al. in 1959 [15] using the height ratio between the crystalline intensity, expressed as the difference ($I_{200} - I_{am}$) and the total intensity (I_{200}), Equation (1). Diffractograms were baseline-corrected with the X Powder software and consequently analyzed using the Perkin Elmer Spectrum v.5.3.1 software with no further processing of peak heights at the (200) plane and at the amorphous region. The total intensity that corresponds to both crystalline and amorphous material (I_{200}), is assigned at $2\theta \sim 25.60^\circ$, whereas the amorphous intensity (I_{am}) is assigned at $2\theta \sim 20.60^\circ$, angles corresponding to Cobalt source radiation.

$$\%CrI = \frac{I_{(200)} - I_{am}}{I_{(200)}} \times 100 \quad (1)$$

The apparent crystallite size L (in nm) was estimated using the Scherrer Equation (2) [16], where K is the Scherrer constant, for which, the value of 0.94 was typically adopted; λ is the X-ray wavelength (1.78897 Å for Co $K\alpha_1$ radiation); β is the full width at half maximum (FWHM) of the diffraction band calculated after curve deconvolution using the Thermo GRAMS suite v.9.0 at the ~11–30.5 2θ range using a 1:1 Gaussian-Lorentzian profile; and θ is the Bragg angle corresponding to the (200) plane.

$$L = \frac{K \times \lambda}{\beta \times \cos\theta} \quad (2)$$

2.4. Proximate Analysis

Proximate analysis was implemented on charred and semi-charred wood samples according to ASTM D1762-84. Samples were air-dried to a constant weight at 21 °C and 65% RH. They were then grounded manually with the use of an agate mortar and pestle, to ~100 µm (No 140-mesh size). Determination of moisture, ash, volatile matter, and fixed carbon was duplicated.

For moisture, approximately 1 g of each condition was placed in a porcelain crucible and weighed to the nearest 0.1 mg. Crucibles and covers were previously dried in a muffle furnace at 750 °C for 10 min and cooled in a desiccator for 1 h. Crucibles containing grounded samples were then placed uncovered in an oven at 105 °C for 2 h. Dried samples were cooled covered in a desiccator for 1 h and weighed. Samples were considered oven-dried when the decrease in weight was ≤ 0.0005 g. Succeeding drying periods were 1 h. Moisture content was calculated based on Equation (3).

$$\text{Moisture}\% = [(A - B)/A] \times 100 \quad (3)$$

where A = grams of air-dry sample used, and B = grams of sample after drying at 105 °C.

For volatile matter, crucibles with lids in place and containing the samples used for moisture determination were placed in a muffle furnace heated to 950 °C. They were first positioned, with the furnace door open, for 2 min on the outer ledge of the furnace (300 °C),

then for 3 min on the edge of the furnace (500 °C) and finally to the rear of the furnace for 6 min with the muffle door closed. Samples were then cooled in a desiccator for 1 h and weighed. The percentage of volatile matter in the sample was calculated based on the Equation (4)

$$\text{Volatile matter}\% = [(B - C)/B] \times 100 \quad (4)$$

where C = grams of sample after drying at 950 °C.

For ash, lids and uncovered crucible used for the volatile matter determination containing the samples were placed in a muffle furnace at 750 °C for 6 h. Samples were cooled with lids in place covered in a desiccator for 1 h and weighed. Samples were repeatedly burned with succeeding 1-h periods until results showed loss of less than 0.0005 g.

The percentage of ash content was calculated based on the Equation (5)

$$\text{Ash}\% = (D/B) \times 100 \quad (5)$$

where D = grams of residue.

Fixed carbon was calculated on a dry basis according to ASTM E870–82 based on the Equation (6).

$$\text{Fixed Carbon}\% = 100 - [\text{Volatile Matter}\% + \text{Ash}\%] \quad (6)$$

3. Results and Discussion

3.1. EDS

Bulk analysis of uncharred, semi-charred, and charred material (Figure 1a,b) showed the presence of aluminum (Al), calcium (Ca), magnesium (Mg), and silica (Si) (Figure 1c). Moreover, both sulfur (S) and iron (Fe) concentrations were shown to decrease in charred areas. This is more likely owed to the different porosity/permeability of the material, which is charring-dependent [17] and that did not allow Fe found in the burial environment [18,19] and S produced by the action of sulfate-reducing bacteria [18] to penetrate into the material uniformly.

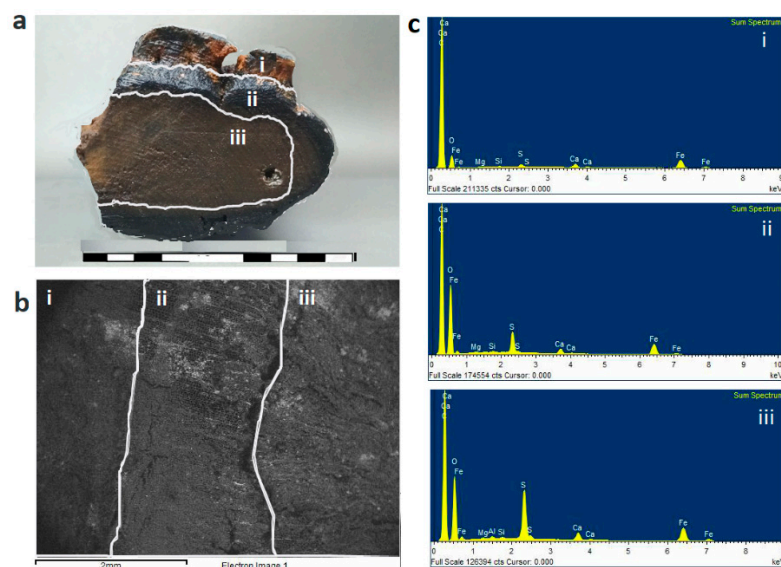


Figure 1. Macroscopic image (a) and SEM micrograph (b) of a sample where charred (i), semi-charred (ii), and uncharred (iii) material coexisted; (c) EDS spectrum of each condition.

Elemental mapping and line scans on samples where all conditions coexisted (Figure 2) also confirmed that the presence of S and Fe is more intense in uncharred areas. Moreover, mapping revealed the coexistence of S and Fe in some spots, which possibly indicates their co-occurrence in the same compound [20,21]. This concurrent presence of S and

Fe in the material is expected to cause severe post-excavation and post-conservation problems [20–23].

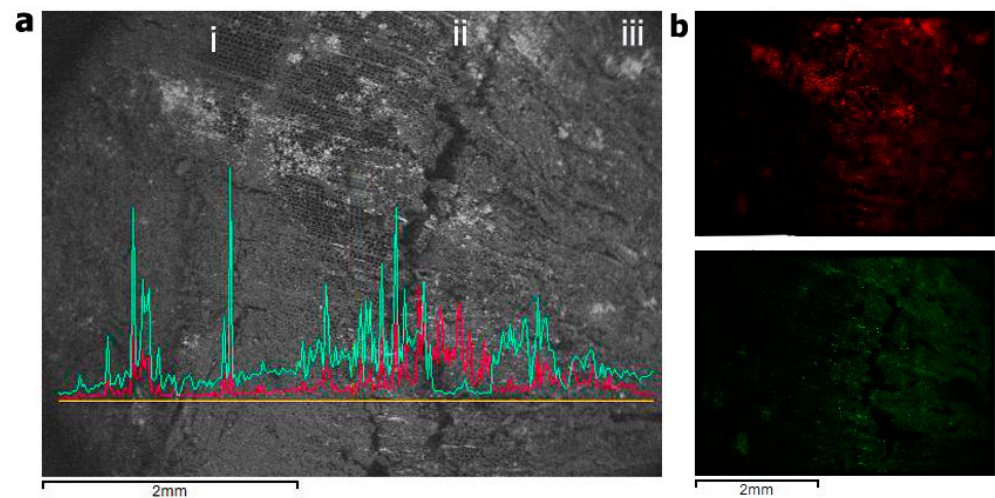


Figure 2. EDS line-scan and mapping of a sample where all conditions coexisted. (a) Line scan of Fe (red) and S (green) (left to right the transition from charred to uncharred, i–iii); (b) mapping of Fe (red) and S (green).

Another find revealed by EDS was the different concentration of carbon (C) and oxygen (O_2) due to charring (Figure 3). As expected, C percentage increases in charred material [17,24,25] while O decreases [17,24]. The increase/decrease rate of C and O is dependent on both temperature and heating duration [17]. Moreover, the relative concentrations of these two elements (Figure 3a) showed that in charred material carbon is much higher than oxygen, indicating that oxygen-containing organic moieties such as polysaccharides and lignin are depleted [26,27]. In contrast, in uncharred areas the ratio of O to C is constant but relatively low, indicating the presence of organic matter, most likely lignin [27], which is in accordance with FTIR results.

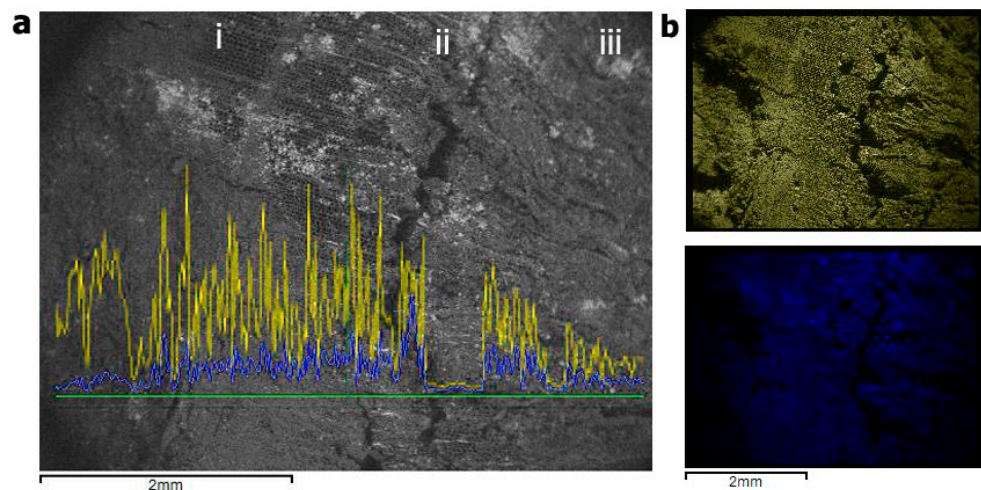


Figure 3. EDS Line-scan and mapping of a sample where all conditions coexisted. (a) Line scan of carbon (yellow) and oxygen (blue) (left to right the transition from charred to uncharred, i–iii); (b) mapping of carbon (yellow) and oxygen (blue).

3.2. FTIR

Spectra obtained from uncharred, semi-charred, and charred archaeological samples along with reference spectra of *Pinus halepensis* and *Pinus brutia* are presented in Figure 4.

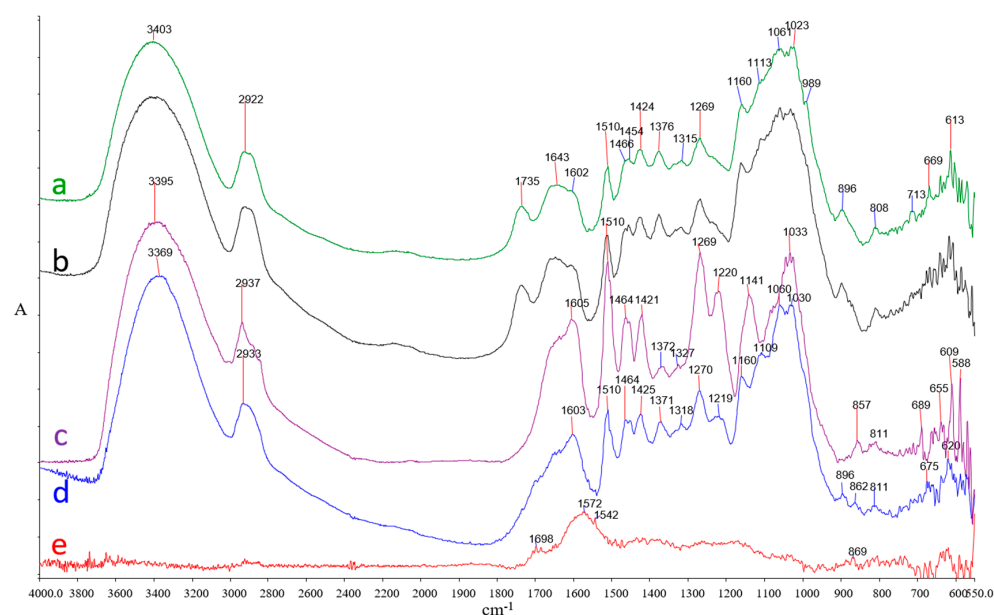


Figure 4. Spectra obtained for reference samples, (a) *Pinus halepensis* and (b) *Pinus brutia* (c) uncharred (d) semi-charred, and (e) charred archaeological samples.

The charred archaeological sample infrared spectrum (Figure 4e) appears typical to charcoals where the broad band at 3400–3320 cm^{-1} representing the –OH stretching vibration of water and the peaks at 3000–2800 cm^{-1} , due to aliphatic C–H stretching vibration derived from methyl, methylene, and methine group, are absent, as these bands decrease in intensity with increasing temperature [11,13,28,29]. Moreover, specific bands assigned to wood components such as hemicelluloses ($\sim 1737 \text{ cm}^{-1}$), lignin (~ 1510 and 1269 cm^{-1}) and cellulose (1026 and $\sim 898 \text{ cm}^{-1}$) [23] and generally all bands in the “fingerprint” region 1500–900 cm^{-1} [23,28] are absent, displaying the chemical changes caused by pyrolysis as well [29]. Nonetheless, the charred sample spectrum presents broad bands at $\sim 1708 \text{ cm}^{-1}$, due to the acidic C=O groups, characteristic of low temperature charcoals’ spectra [11,13] and a broad band at 1610–1590 cm^{-1} due to lignin aromatic C=C skeletal vibrations, which have been also reported to increase in intensity with increasing charring [29].

Semi-charred material spectrum appears comparable to spectra of thermally modified wood. The intensity of hemicelluloses ester carbonyl peak at 1737 cm^{-1} is evidently decreased, as most of the xylan-linked acetyl groups are expected to be cleaved with increasing temperature and time during the burning of wood [30–34]. The cellulose peak at $\sim 895 \text{ cm}^{-1}$ due to C–H deformations at the glycosidic linkage was also decreased, which has been reported to occur when wood is exposed to heat [32,33,35]. It should be mentioned though, that part of carbohydrates’ reduction could be owed to abiotic or biotic processes occurring in the marine environment during the service life of the ship or during burial [36–38]. Other carbohydrate bands at ~ 1371 , ~ 1160 , and 1110 cm^{-1} showed no significant difference in intensity. Similarly, the major lignin bands, approximately at 1603, 1510, 1464, 1425, 1371, 1316, 1269, and 1223 cm^{-1} showed no intensity differences as reported for thermally modified wood [33] whereas the slight rise observed for some (1603, 1510, and 1425 cm^{-1}) is mainly due to the increase in relative lignin content [35]. Nonetheless, an increase in absorption at 1030 and 1060 cm^{-1} has been observed indicating respectively the pronounced aromatic nature of the semi-charred wood, since this absorption band also indicates aromatic in-plane C–H deformation and changes in cellulose structure [34,35] along with the formation of aliphatic alcohols during heating [31,35].

The spectrum of uncharred waterlogged wood appears typical of biodeteriorated waterlogged wood, where significantly pronounced lignin bands 1605, 1510, 1269, and 1220 cm^{-1} appear with a corresponding decrease in the intensities of carbohydrate bands at 1737, 1370, 1158, and 895 cm^{-1} . More specifically, it is indicated that shipwreck timbers

have been deteriorated by erosion bacteria or/and soft-rot fungi, which thrive in the marine environment [37]. Erosion bacteria decay has been often reported to be associated with lignin bands' increment and carbohydrates bands' decrement [38,39]. Soft-rotters also degrade carbohydrates in preference to lignin [37] and most of them are unable to degrade guaiacyl lignin, found predominantly in softwoods, with the exception of the cavity-forming species [40]. This probably explains the new band developed at $\sim 1140\text{ cm}^{-1}$, which in combination with the decrease in the intensity at 1060 and the increase at 1030 cm^{-1} , may be attributable to the guaiacyl lignin relative increase compared to carbohydrates [41] (C–H deformation in the guaiacyl unit, with C–O deformation in primary alcohol). This is also in accordance with another band present in uncharred wood sample at $\sim 855\text{ cm}^{-1}$ that is associated with the C–H out-of-plane vibrations in guaiacyl lignin [42].

3.3. XRD

Diffractograms regarding the (110), (110), (102), (200), and (004) reflections of the two reference samples (*P. halepensis* and *P. brutia*) along with charred, semi-charred, and uncharred archaeological waterlogged samples are shown in Figure 5. Both reference samples and semi-charred diffractograms showed all peaks typical of reflection planes of wood cellulose [43–45]. In contrast, the uncharred sample diffractogram showed a considerably flattened line-shape; nonetheless, it showed a more prominent peak on the (200) plane reflection with respect to the (110) and (110). The charred sample diffractogram, as reported by other researchers [46], appeared also flattened with a weak and broad peak regarding the (200) reflection plane, with a shifted vague maximum at $\sim 30^\circ$.

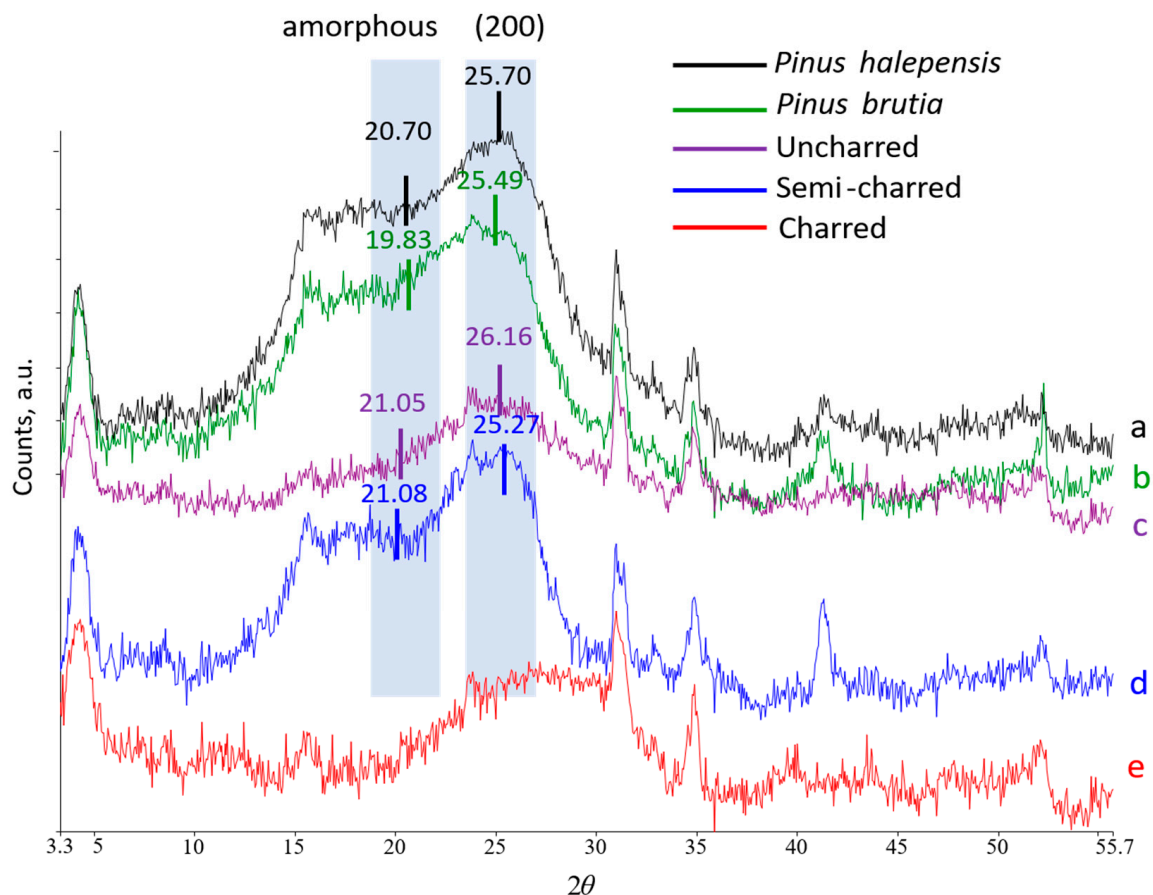


Figure 5. X-ray diffraction pattern of (a) *Pinus halepensis* and (b) *Pinus brutia* reference samples in comparison with (c) uncharred, (d) semi-charred, and (e) charred waterlogged samples. The 2θ values correspond to Cobalt source reflections.

Crystallinity index (CrI) of the material examined varied greatly depending on the charring degree (Table 1). The higher cellulose CrI value was calculated for the uncharred material, and followed by semi-charred wood and by controls. However, CrI values were not in accordance with the respective crystallite sizes (L), as for the uncharred material, L presented the lowest value.

Table 1. Band positions of the maximum total intensity (I_{200}) and the minimum intensity of the amorphous cellulose (I_{am}). CrI represents the crystalline index based on Segal's method and L correspond to the crystallite size.

Sample	2θ (I_{200}) ^a	2θ (I_{am}) ^a	CrI	L (nm)
<i>Pinus brutia</i>	25.49	19.83	41.7%	2.29
<i>Pinus halepensis</i>	25.70	20.70	41.8%	2.51
Semi-charred	25.27	21.08	47.4%	2.75
Uncharred	26.16	21.05	53.2%	1.10
Charred ^b	-	-	-	-

^a 2θ values are expressed as Co-source. ^b CrI was not calculated as no cellulose is expected to be preserved with charring above 400 °C.

The considerably high CrI of uncharred material was not anticipated, as in archaeological wood the crystallinity usually decreases with decay [23,47–49]. Nonetheless, crystallinity's increase has been reported by other authors in initial stages of degradation due to the dramatic loss of amorphous cellulose regions [23,48,50]. It is believed though that this explanation does not justify the high CrI values of uncharred material as the diffractogram line-shape, the FTIR results and the lowest crystallite size (L) recorded point out to a material in which cellulose is probably completely destroyed. Therefore, it appears that the Segal method for CrI calculation cannot successfully apply to severely deteriorated material. This could be due to several reasons related to the deficiency of the Segal method [44,51,52]; nonetheless, it is considered that is principally owed to the highly depleted cellulose fraction. It is recommended for this type of material to use other methods such as the two-dimensional X-ray diffraction.

The relative higher CrI of semi-charred material compared to references is considered that is due to amorphous cellulose degradation, which occurs during the initial stages of heating and progresses as the heat temperature rises [53–55]. This is in accordance with the high L value that corresponds to relatively larger crystal that the other materials examined. Moreover, indicates that the charring temperature for semi-charred material was lower than ~300 °C as above this threshold, cellulose crystalline part is expected to degrade severely [46,56].

3.4. Proximate Analysis

Proximate analysis' results on moisture content, volatile matter, ash content and fixed carbon are presented in Table 2 for both semi-charred and charred conditions. For the moisture content, no difference was recorded among samples. As it was anticipated, the volatile matter was lower in fully charred material as it is negatively correlated with temperature [57–59]. Similar values for volatile matter have been recorded by Dias Junior et al. (2020) [59] indicating combustion at/over 450 °C. The difference of volatile matter between the two conditions can be attributed to the barrier role of charred layer over the inner areas [60,61].

Table 2. Proximate analysis results for charred and semi-charred samples. Percentages values of moisture content, volatile matter, ash content and fixed carbon are the average of 2 replicates. Fixed carbon was calculated on dry basis.

Sample	Moisture Content	Volatile Matter	Ash Content	Fixed Carbon
Semi-charred	6.53	75.07	1.87	16.51
Charred	6.71	24.16	3.53	65.59

Ash content appears to increase with combustion as expected [57,58]. Likewise, fixed carbon content appears to increase as combustion progresses and it is in accordance with results of other researchers [57–59] and with the EDS results obtained in the present study. This increase is suggested to be a result of pyrolytic process which favors the volatile removal and consequently the elevation of ash-minerals and carbon [57].

4. Conclusions

This work demonstrated major chemical differences among shipwreck timbers' due to charring. Three distinct conditions, consisting of uncharred, semi-charred, and charred wood, were documented which were directly related to the fire heat flux (temperature and duration) and the surrounding oxygen concentration.

Regarding the organic chemistry of the archaeological material, charred samples showed an analogous profile to charcoals, where both polysaccharides and lignin were almost absent due to pyrolysis. Semi-charred material showed a chemical similarity to thermally modified wood, where hemicelluloses were reduced, cellulose crystallinity was increased, and lignin showed no large differences compared to sound wood. Uncharred waterlogged wood chemistry was analogous to biodeteriorated wood, as carbohydrates were dramatically depleted, and the relative lignin content appeared increased.

The inorganic chemistry of the archaeological wood, based on elements' concentrations and topography also varied among the three conditions. Sulfur and iron concentrations were found increased in uncharred areas and their topochemistry indicated their possible co-existence in the same compounds. This concurrent presence of S and Fe it is considered that has the potential to cause severe post-excavation problems.

Finally, proximate analysis also demonstrated differences among conditions, as ash content and fixed carbon was higher in charred compared to semi-charred samples.

All chemical differences documented are awaited to be taken into consideration when developing the conservation plan of this shipwreck, as it is anticipated to influence not only conservation methods' efficacy but also the post-treatment behavior of the material.

It is believed, however, that further investigation is required in order to correlate this diverse chemistry to physical properties such as porosity, permeability, density, and shrinkage, in order to provide a more practical contribution to the shipwreck conservation.

Author Contributions: Conceptualization: A.P.; data curation: E.M., S.B. and A.P.; formal analysis: E.M. and S.B.; investigation: E.M., S.B. and A.P.; methodology: E.M., S.B. and A.P.; Supervision: A.P. All authors have read and agreed to the published version of the manuscript.

Funding: This research received no external funding.

Acknowledgments: The authors would like to thank G. Koutsouflakis, for providing the archaeological material and A. Karabotsos for his assistance with the SEM-EDS analysis.

Conflicts of Interest: The authors declare no conflict of interest.

References

1. Koutsouflakis, G.; Rieth, E. A late-12th-century byzantine shipwreck in the port of Rhodes A preliminary report. In *Under the Mediterranean I Studies in Maritime Archaeology*; Demesticha, S., Blue, L., Eds.; Sidestone Press: Leiden, The Netherlands, 2021.
2. Koutsouflakis, G. Three shipwrecks of the medieval era in the commercial port of Rhodes. In *Proceedings of the Archeological Work in Aegean Islands, Lesbos, Greece, 27 November–1 December 2013*; Birtacha, K., Triantaphyllidis, P., Sarantidis, K., Eds.; pp. 477–500.
3. Mitsi, E.; Pournou, A. Conserving a charred medieval shipwreck: A preliminary study. In *Proceedings of the 14th ICOM-CC WOAM Conference, Portsmouth, UK, 20–24 May 2019*.
4. Stamm, A.J. Thermal degradation of wood and cellulose. *Ind. Eng. Chem.* **1956**, *48*, 413–417. [[CrossRef](#)]
5. Shafizadeh, F. The chemistry of pyrolysis and combustion. *Adv. Chem.* **1984**, *207*, 489–529.
6. Meincken, M.; Smit, N.H.; Steinmann, D. Physical properties of burnt timber, with special focus on the drying performance. *Eur. J. Wood Wood Prod.* **2015**, *68*, 455–461. [[CrossRef](#)]
7. Bartlett, A.I.; Hadden, R.M.; Bisby, L.A. A review of factors affecting the burning behaviour of wood for application to tall timber construction. *Fire Technol.* **2019**, *55*, 1–49. [[CrossRef](#)]
8. Kollmann, F.F.; Côté, W.A. *Principles of Wood Science and Technology. Vol. I. Solid Wood*; Springer: Berlin/Heidelberg, Germany, 1968; ISBN 9783642879302.
9. Friquin, K.L. Material properties and external factors influencing the charring rate of solid wood and glue-laminated timber. *Fire Mater.* **2011**, *35*, 303–327. [[CrossRef](#)]
10. Liu, Q.; Wang, S.R.; Fang, M.X.; Luo, Z.Y.; Cen, K.F.; Chow, W.K. Bench-scale studies on wood pyrolysis under different environments. *Fire Saf. Sci.* **1994**, *7*, 94.
11. Guo, Y.; Bustin, R. FTIR spectroscopy and reflectance of modern charcoals and fungal decayed woods: Implications for studies of inertinite in coals. *Int. J. Coal Geol.* **1998**, *37*, 29–53. [[CrossRef](#)]
12. White, R.H.; Dietenberger, M. Wood products: Thermal degradation and fire. *Encycl. Mater. Sci. Technol.* **2001**, 9712–9716. [[CrossRef](#)]
13. Constantine, M.; Mooney, S.; Hibbert, B.; Marjo, C.; Bird, M.; Cohen, T.; Forbes, M.; Mcbeath, A.; Rich, A.; Stride, J. Science of the Total Environment Using charcoal, ATR FTIR and chemometrics to model the intensity of pyrolysis: Exploratory steps towards characterising fire events. *Sci. Total Environ.* **2021**, *783*, 147052. [[CrossRef](#)]
14. Hill, C.A.S. Modifying the properties of wood. In *Wood Modification: Chemical, Thermal and Other Processes*; John Wiley & Sons: Hoboken, NJ, USA, 2006; pp. 19–44. ISBN 9780470021729.
15. Segal, L.; Creely, J.J.; Martin, A.E., Jr.; Conrad, C.M. An empirical method for estimating the degree of crystallinity of native cellulose using the X-ray diffractometer. *Text. Res. J.* **1959**, *29*, 786–794. [[CrossRef](#)]
16. Scherrer, P.; Debye, P. Bestimmung der grösse und der inneren struktur von kolloidteilchen mittels röntgensahlen [determination of the size and internal structure of colloidal particles using X-rays]. *Nachr. Ges. Wiss. Göttingen Math.-Physik. Kl.* **1918**, *2*, 101–120.
17. Rutherford, D.; Wershaw, R.; Cox, L. *Changes in Composition and Porosity Occurring during the Thermal Degradation of Wood and Wood Components: U.S. Geological Survey Scientific Investigations Report 2004-5292*; U.S. Geological Survey: Reston, VA, USA, 2005; Volume 79.
18. Sandström, M.; Jalilvand, F.; Persson, I.; Fors, Y.; Damian, E.; Gelius, U.; Hall-Roth, I.; Dal, L.; Richards, V.L.; Godfrey, I. The sulphur threat to marine archaeological artefacts: Acid and iron removal from the Vasa. In *Proceedings of the Conservation Science 2002, Edinburgh, UK, 22–24 May 2002*; pp. 79–87.
19. Monachon, M.; Albelda-Berenguer, M.; Pelé, C.; Cornet, E.; Guilminot, E.; Rémazeilles, C.; Joseph, E. Characterization of model samples simulating degradation processes induced by iron and sulfur species on waterlogged wood. *Microchem. J.* **2020**, *155*, 104756. [[CrossRef](#)]
20. Fors, Y. Sulfur-Related Conservation Concerns for Marine Archaeological Wood. Ph.D. Thesis, Stockholm University, Stockholm, Sweden, 2008.
21. Rémazeilles, C.; Tran, K.; Guilminot, E.; Conforto, E.; Refait, P. Study of Fe (II) sulphides in waterlogged archaeological wood. *Stud. Conserv.* **2013**, *58*, 297–307. [[CrossRef](#)]
22. Fors, Y.; Nilsson, T.; Risberg, E.D.; Sandström, M.; Torssander, P. Sulfur accumulation in pinewood (*Pinus sylvestris*) induced by bacteria in a simulated seabed environment: Implications for marine archaeological wood and fossil fuels. *Int. Biodeterior. Biodegrad.* **2008**, *62*, 336–347. [[CrossRef](#)]
23. High, K.E.; Penkman, K.E.H. A review of analytical methods for assessing preservation in waterlogged archaeological wood and their application in practice. *Herit. Sci.* **2020**, *8*, 1–34. [[CrossRef](#)]
24. Valenzuela-Calahorra, C.; Bernalte-García, A.; Gómez-Serrano, V.; Bernalte-García, M.J. Influence of particle size and pyrolysis conditions on yield, density and some textural parameters of chars prepared from holm-oak wood. *J. Anal. Appl. Pyrolysis* **1987**, *12*, 61–70. [[CrossRef](#)]
25. Todaro, L.; Rita, A.; Cetera, P.; D’Auria, M. Thermal treatment modifies the calorific value and ash content in some wood species. *Fuel* **2015**, *140*, 1–3. [[CrossRef](#)]
26. Inari, G.N.; Petrissans, M.; Lambert, J.; Ehrhardt, J.J.; Gérardin, P. XPS characterization of wood chemical composition after heat-treatment. *Surf. Interface Anal.* **2006**, *38*, 1336–1342. [[CrossRef](#)]

27. Kocaefe, D.; Huang, X.; Kocaefe, Y.; Boluk, Y. Quantitative characterization of chemical degradation of heat-treated wood surfaces during artificial weathering using XPS. *Surf. Interface Anal.* **2013**, *45*, 639–649. [[CrossRef](#)]
28. Poletto, M.; Zattera, A.J.; Santana, R.M.C. Structural differences between wood species: Evidence from chemical composition, FTIR spectroscopy, and thermogravimetric analysis. *J. Appl. Polym. Sci.* **2012**, *126*, E336–E343. [[CrossRef](#)]
29. Tintner, J.; Preimesberger, C.; Pfeifer, C.; Soldo, D.; Ottner, F.; Wriessnig, K.; Rennhofer, H.; Lichtenegger, H.; Novotny, E.H.; Smidt, E. Impact of pyrolysis temperature on charcoal characteristics. *Ind. Eng. Chem. Res.* **2018**, *57*, 15613–15619. [[CrossRef](#)]
30. Tjeerdsma, B.F.; Militz, H. Chemical changes in hydrothermal treated wood: FTIR analysis of combined hydrothermal and dry heat-treated wood. *Holz Roh-Und Werkst.* **2005**, *63*, 102–111. [[CrossRef](#)]
31. Popescu, M.-C.; Froidevaux, J.; Navi, P.; Popescu, C.-M. Structural modifications of *Tilia cordata* wood during heat treatment investigated by FT-IR and 2D IR correlation spectroscopy. *J. Mol. Struct.* **2013**, *1033*, 176–186. [[CrossRef](#)]
32. Esteves, B.; Marques, A.V.; Domingos, I.; Pereira, H. Chemical changes of heat treated pine and eucalypt wood monitored by FTIR. *Maderas. Cienc. Tecnol.* **2013**, *15*, 245–258. [[CrossRef](#)]
33. Özgenç, Ö.; Durmaz, S.; Boyacı, İ.H.; Eksi-Koçak, H. ATR-FTIR spectroscopic analysis of thermally modified wood degraded by rot fungi. *Drewno* **2018**, *61*. [[CrossRef](#)]
34. Kubovsk, I.; Ka, D. Structural changes of oak wood main components caused by thermal modification. *Polymers* **2020**, *12*, 485. [[CrossRef](#)]
35. Kotilainen, R.A.; Toivanen, T.-J.; Alén, R.J. FTIR monitoring of chemical changes in softwood during heating. *J. Wood Chem. Technol.* **2000**, *20*, 307–320. [[CrossRef](#)]
36. Kim, Y.S. Short note: Chemical characteristics of waterlogged archaeological wood. *Holzforschung* **1990**, *44*, 169–172. [[CrossRef](#)]
37. Pournou, A. Wood deterioration by aquatic microorganisms. In *Biodeterioration of Wooden Cultural Heritage: Organisms and Decay Mechanisms in Aquatic and Terrestrial Ecosystems*; Pournou, A., Ed.; Springer International Publishing: Cham, Switzerland, 2020; pp. 177–260. ISBN 978-3-030-46504-9.
38. Pedersen, N.B.; Gierlinger, N.; Thygesen, L.G. Bacterial and abiotic decay in waterlogged archaeological *Picea abies* (L.) Karst studied by confocal Raman imaging and ATR-FTIR spectroscopy. *Holzforschung* **2015**, *69*, 103–112. [[CrossRef](#)]
39. Gelbrich, J.; Mai, C.; Militz, H. Chemical changes in wood degraded by bacteria. *Int. Biodeterior. Biodegrad.* **2008**, *61*, 24–32. [[CrossRef](#)]
40. Nilsson, B.T.; Daniel, G.; Kirk, T.K.; Obst, J.R.; Service, F. Chemistry and microscopy of wood decay by some higher ascomycetes. *Holzforschung* **1989**, *43*, 11–18. [[CrossRef](#)]
41. Pandey, K.; Pitman, A. FTIR studies of the changes in wood chemistry following decay by brown-rot and white-rot fungi. *Int. Biodeterior. Biodegrad.* **2003**, *52*, 151–160. [[CrossRef](#)]
42. Traoré, M.; Kaal, J.; Cortizas, A.M. Differentiation between pine woods according to species and growing location using FTIR-ATR. *Wood Sci. Technol.* **2018**, *52*, 487–504. [[CrossRef](#)] [[PubMed](#)]
43. Andersson, S.; Wikberg, H.; Pesonen, E.; Maunu, S.L.; Serimaa, R. Studies of crystallinity of Scots pine and Norway spruce cellulose. *Trees* **2004**, *18*, 346–353. [[CrossRef](#)]
44. Park, S.; Baker, J.O.; Himmel, M.E.; Parilla, P.A.; Johnson, D.K. Cellulose crystallinity index: Measurement techniques and their impact on interpreting cellulase performance. *Biotechnol. Biofuels* **2010**, *3*, 10. [[CrossRef](#)]
45. Agarwal, U.P.; Reiner, R.R.; Ralph, S.A.; Forest, A.; Gi, O.; Drive, P. Estimation of cellulose crystallinity of lignocelluloses using near-IR. *J. Agric. Food Chem.* **2013**, *61*, 103–113. [[CrossRef](#)]
46. Kwon, S.-M.; Kim, N.-H.; Cha, D.-S. An investigation on the transition characteristics of the wood cell walls during carbonization. *Wood Sci. Technol.* **2009**, *43*, 487–498. [[CrossRef](#)]
47. Giachi, G.; Bettazzi, F.; Chimichi, S.; Staccioli, G. Chemical characterisation of degraded wood in ships discovered in a recent excavation of the Etruscan and Roman harbour of Pisa. *J. Cult. Herit.* **2003**, *4*, 75–83. [[CrossRef](#)]
48. Popescu, C.-M.; Larsson, P.T.; Tibirna, C.M.; Vasile, C. Characterization of fungal-degraded lime wood by X-ray diffraction and cross-polarization magic-angle-spinning ¹³C-nuclear magnetic resonance spectroscopy. *Appl. Spectrosc.* **2010**, *64*, 1054–1060. [[CrossRef](#)]
49. Zhou, Y.; Wang, K.; Hu, D. Degradation features of archaeological wood surface to deep inside a case study on wooden boards of marquis of Haihun’s outer coffin. *Wood Res.* **2018**, *63*, 419–430.
50. Howell, C.; Hastrup, A.C.S.; Goodell, B.; Jellison, J. Temporal changes in wood crystalline cellulose during degradation by brown rot fungi. *Int. Biodeterior. Biodegrad.* **2009**, *63*, 414–419. [[CrossRef](#)]
51. Thygesen, A.; Oddershede, J.; Lilholt, H.; Thomsen, A.B.; Ståhl, K. On the determination of crystallinity and cellulose content in plant fibres. *Cellulose* **2005**, *12*, 563–576. [[CrossRef](#)]
52. French, A.D.; Cintron, M.S. Cellulose polymorphism, crystallite size, and the segal crystallinity index. *Cellulose* **2013**, *20*, 583–588. [[CrossRef](#)]
53. Sivonen, H.; Maunu, S.L.; Sundholm, F.; Jämsä, S.; Viitaniemi, P. Magnetic resonance studies of thermally modified wood. *Holzforschung* **2002**, *56*, 648–654. [[CrossRef](#)]
54. Esteves, B.M.; Pereira, H.M. Wood modification by heat treatment: A review. *BioResources* **2009**, *4*, 370–404. [[CrossRef](#)]
55. Tarmian, A.; Mastouri, A. Changes in moisture exclusion efficiency and crystallinity of thermally modified wood with aging. *iFor.-Biogeosci. For.* **2019**, *12*, 92–97. [[CrossRef](#)]

56. Wang, S.; Dai, G.; Ru, B.; Zhao, Y.; Wang, X.; Xiao, G. Influence of torrefaction on the characteristics and pyrolysis behavior of cellulose. *Energy* **2017**, *120*, 864–871. [[CrossRef](#)]
57. Fuwape, J.A. Effects of carbonisation temperature on charcoal from some tropical trees. *Bioresour. Technol.* **1996**, *57*, 91–94. [[CrossRef](#)]
58. Ruiz-aquino, F.; Ruiz-ángel, S.; Sotomayor-castellanos, J.R. Energy characteristics of wood and charcoal of selected tree species in Mexico. *Wood Res.* **2019**, *64*, 71–82.
59. Dias Junior, A.F.; Esteves, R.P.; Da Silva, Á.M.; Sousa Júnior, A.D.; Oliveira, M.P.; Brito, J.O.; Napoli, A.; Braga, B.M. Investigating the pyrolysis temperature to define the use of charcoal. *Eur. J. Wood Wood Prod.* **2020**, *78*, 193–204. [[CrossRef](#)]
60. Mikkola, E. Charring of Wood Based Materials. *Fire Saf. Sci.* **1991**, *3*, 547–556. [[CrossRef](#)]
61. Lowden, L.A.; Hull, T.R. Flammability behaviour of wood and a review of the methods for its reduction. *Fire Sci. Rev.* **2013**, *2*, 4. [[CrossRef](#)]